Liquid state isomorphism, Rosenfeld-Tarazona temperature scaling and Riemannian thermodynamic geometry

Peter Mausbach
Technical University of Cologne, 50678 Köln/Germany

Andreas Köster and Jadran Vrabec*
Thermodynamics and Energy Technology, University of Paderborn, 33098 Paderborn/Germany
(Dated: May 28, 2018)

Aspects of isomorph theory, Rosenfeld-Tarazona temperature scaling and thermodynamic geometry are comparatively discussed on the basis of the Lennard-Jones potential. The first two approaches approximate the high density fluid state well when the repulsive interparticle interactions become dominant, which is typically the case close to the freezing line. However, previous studies of Rosenfeld-Tarazona scaling for the isochoric heat capacity and its relation to isomorph theory reveal deviations for the temperature dependence. It turns out that a definition of a state region in which repulsive interactions dominate is required for achieving consistent results. The Riemannian thermodynamic scalar curvature R allows for such a classification, indicating predominantly repulsive interactions by $R > 0$. An analysis of the isomorphic character of the freezing line and the validity of Rosenfeld-Tarazona temperature scaling show that these approaches are consistent only in a small state region.

* Corresponding author. E-mail address: jadran.vrabec@upb.de

I. INTRODUCTION

The thermodynamic behavior of the high density fluid phase has attracted a lot of interest in the recent past. New theoretical approaches [1–5] reveal features that bear important information for the understanding of this state region. Of particular importance for these investigations are so-called simple liquids that are characterized by isotropic interparticle interactions. Based on the presence of strong correlations between potential energy and virial, a new definition of simple liquids has recently been proposed [6–9]: Strongly correlating liquids, also called Roskilde-simple liquids, possess universal curves along which several properties are invariant when expressed in terms of appropriately reduced thermodynamic variables as described by isomorph theory [1]. Another aspect of the high density fluid phase was investigated by Rosenfeld and Tarazona (RT) [4]. Their theoretical arguments are based on thermodynamic perturbation theory, using a bulk hard-sphere reference system, and reveal a simple $T^{3/5}$ temperature scaling relation for the potential energy (residual internal energy) of liquids. Moreover, in the respective state region, Bolmatov et al. [3, 10] studied a dynamic transition between gas-like and liquid-like behavior along the so-called Frenkel line that is characterized by the disappearance of solid-like oscillations in particle dynamics.

Frequently, the question is raised to what extent similarities between these approaches exist and which physical fundamentals they may have. A contribution to this discussion was made by Ingebrigtsen et al. [11] who assessed the accuracy of the RT temperature scaling ($T^{-2/5}$) for the residual isochoric heat capacity of 18 model liquids. By applying statistical measures, they have shown that RT scaling is closely obeyed by Roskilde-simple liquids. However, experimental data for argon exhibit deficiencies of the RT approach at high temperatures [11].

The present study analyzes to which extent isomorph theory and RT scaling may be considered as good approximations depending on the state region. Both rely on the dominance of repulsive interactions. A direct measure for the interaction strength is the Riemannian scalar curvature R, which is an element of thermodynamic metric geometry [12]. The sign of R is associated with the character of interparticle interactions [13]: $R > 0$, if repulsive interactions dominate, e.g. in solids, and $R < 0$, if attractive interactions dominate, e.g. in the critical region. This relatively new approach is introduced into the present discussion because investigations of R allow for the identification of state

regions in which fluid theories, relying on the dominance of repulsive interactions, may be applied successfully.

The present study is limited to simple liquids whose interactions are described by Lennard-Jones (LJ) potential. As a standard model in molecular simulation studies, the LJ potential is commonly used to represent spherical, nonpolar molecules [14]. Furthermore, it is an important model for studying phase equilibria [15], phase change processes [16, 17], clustering behavior [18], or transport [19] and interface properties [20] of simple fluids. The LJ potential is commonly expressed as

$$u_{\mathrm{LJ}} = 4\varepsilon \left[\left(\frac{\sigma}{r}\right)^{12} - \left(\frac{\sigma}{r}\right)^{6} \right], \tag{1}$$

where σ and ε are size and energy parameters, while r is the distance between two particles. In a recent study, Köster et al. [21] investigated the thermodynamic behavior of the LJ system ranging from the high density fluid to the solid state. They employed the statistical mechanical formalism proposed by Lustig [22, 23] that allows for the concurrent calculation of any partial Helmholtz energy derivative in the canonical (NVT) ensemble within a single simulation run. The large data set provided by Köster et al. [21] served in this work as a basis for thermodynamic information.

This paper is organized as follows: Section II introduces the molecular simulation method used to sample thermodynamic properties for the present analysis. Isomorphic predictions, some of which have not been proven so far, are assessed in section III. The causes of limited applicability of RT temperature scaling are investigated in section IV. A detailed geometric analysis of the considered phase region is performed in section V and its relationship to isomorph theory and RT scaling is discussed. A conclusion sums the present findings up.

II. MOLECULAR SIMULATION METHOD

The statistical mechanical formalism proposed by Lustig [22, 23] is a powerful route for calculating every time independent thermodynamic property in a single simulation run. This is done on the basis of partial derivatives of the total molar Helmholtz energy [24]

$$a(T,\rho) = a^{\mathrm{o}}(T,\rho) + a^{\mathrm{r}}(T,\rho), \tag{2}$$

which is commonly separated into an ideal (superscript "o") and a residual (superscript "r") contribution. The ideal contribution is straightforward for the LJ potential because it is a classical monatomic, whereas the residual contribution is a consequence of the intermolecular interactions. The reduced residual Helmholtz energy derivatives can be written as

$$A_{mn}^{\mathrm{r}} = (1/T)^m \rho^n \frac{\partial^{m+n} a^{\mathrm{r}}(T,\rho)/(R_{\mathrm{G}}T)}{\partial(1/T)^m \partial\rho^n}, \tag{3}$$

wherein T denotes the temperature, ρ the density and R_{G} the ideal gas constant. m and n represent the order of the partial derivative with respect to density and inverse temperature, respectively.

In recent work, Lustig's formalism [22, 23] was implemented into the molecular simulation tool $ms2$ [25–27] up to the order $m = 3$ and $n = 2$. Therefore, eight partial Helmholtz energy derivatives can be sampled simultaneously and subsequently used to calculate common thermodynamic properties. A conversion of all properties that are relevant in this study is given in Table I. However, the method of Lustig does not allow for the direct sampling of entropic properties like A_{00}^{r}, cf. Table I. To overcome this limitation, thermodynamic integration [27] was used.

The present simulations were carried out with $N = 1372$ particles using Monte Carlo (MC) sampling with an acceptance rate [28] of 0.5. Throughout, the cutoff radius was set to be half the edge length of the cubic simulation volume. Each simulation run was thoroughly equilibrated prior to sampling the desired properties for 2 to $3 \cdot 10^6$ cycles, where one cycle corresponds to 1372 translational propagation attempts. More details on the simulation parameters are given in ref. [21]. As usual for studies based on the LJ potential, all thermodynamic data are reported here in a reduced unit system. This reduction is based on the LJ size σ and energy ε parameters, e.g. $T^* = Tk_{\mathrm{B}}/\varepsilon$, $\rho^* = \rho\sigma^3$ and $p^* = p\sigma^3/\varepsilon$, with Boltzmann's constant k_{B} and pressure p. The asterisk will be omitted in the following.

III. LIQUID STATE ISOMORPHISM

About a decade ago, Dyre and coworkers [6–9] discovered the existence of strong correlations between the potential energy (the residual contribution to the internal energy u^r) and the virial w (the residual contribution to the pressure)

TABLE I. Thermodynamic properties in relation to the reduced Helmholtz energy derivatives, where the ideal contributions are $A^{\mathrm{o}}_{10} = -A^{\mathrm{o}}_{20} = 3/2$.

Property	Relation to reduced Helmholtz energy derivatives
pressure $p = -(\partial a/\partial v)_T$	$\frac{p}{\rho R_{\mathrm{G}} T} = 1 + A^{\mathrm{r}}_{01}$
internal energy $u = a - T(\partial a/\partial T)_v$	$\frac{u}{R_{\mathrm{G}} T} = A^{\mathrm{o}}_{10} + A^{\mathrm{r}}_{10}$
isochoric heat capacity $c_v = (\partial u/\partial T)_v$	$\frac{c_v}{R_{\mathrm{G}}} = -A^{\mathrm{o}}_{20} - A^{\mathrm{r}}_{20}$
entropy $s = -(\partial a/\partial T)_v$	$\frac{s}{R_{\mathrm{G}}} = A^{\mathrm{o}}_{10} + A^{\mathrm{r}}_{10} - A^{\mathrm{o}}_{00} - A^{\mathrm{r}}_{00}$
density scaling exponent $\gamma = (\partial \ln T/\partial \ln \rho)_{s^{\mathrm{r}}}$	$\gamma = -\frac{A^{\mathrm{r}}_{01} - A^{\mathrm{r}}_{11}}{A^{\mathrm{r}}_{20}}$
Grüneisen parameter $\gamma_{\mathrm{G}} = (\partial \ln T/\partial \ln \rho)_s$	$\gamma_{\mathrm{G}} = -\frac{1 + A^{\mathrm{r}}_{01} - A^{\mathrm{r}}_{11}}{A^{\mathrm{o}}_{20} + A^{\mathrm{r}}_{20}}$

for a large class of model liquids [29]. For characterization, they employed the correlation coefficient

$$\mathcal{R}(\rho, T) = \frac{\langle \delta u^r \ \delta w \rangle}{\sqrt{\langle (\delta u^r)^2 \rangle \, \langle (\delta w)^2 \rangle}} \ , \tag{4}$$

where $\delta u^r = u^r - \langle u^r \rangle$ and $\delta w = w - \langle w \rangle$. Note that the correlation coefficient $\mathcal{R}$ does not coincide with the Riemannian scalar curvature R. To avoid confusion between several similar abbreviations employed in the literature, an explanatory table is given in the appendix. Because the term residual internal energy follows Lustig's terminology, it is subsequently used instead of potential energy.

Liquids with strong residual internal energy-virial correlations are labeled as Roskilde-simple, if $\mathcal{R}$ is close to unity. Defining a limit is somewhat arbitrary, however, $\mathcal{R} > 0.9$ is commonly accepted [1]. The condition $\mathcal{R} > 0.9$ holds only in a certain region of the phase diagram and therefore requires an evaluation of the correlation coefficient $\mathcal{R}$ in (ρ, T) coordinates. For the LJ fluid, this condition is met in a region starting below the triple point liquid density along a boundary of decreasing density with increasing temperature and ranges up to the freezing line (FL), cf. Fig. 1. Therein, isomorphs can be constructed as curves where the residual entropy s^r [32] is constant, being also referred to as configurational adiabats [33]. A quantity generating constant residual entropy s^r curves is the density scaling exponent γ, cf. Table I. It can be shown that structure and dynamics of Roskilde-simple liquids along isomorphs are invariant, when expressed in specific units [1].

A natural question arising in this context is whether invariances along the FL and melting line (ML) of Roskilde-simple systems exist. Gnan et al. [9] and Schrøder et al. [8] indicated that the FL of the LJ system should be

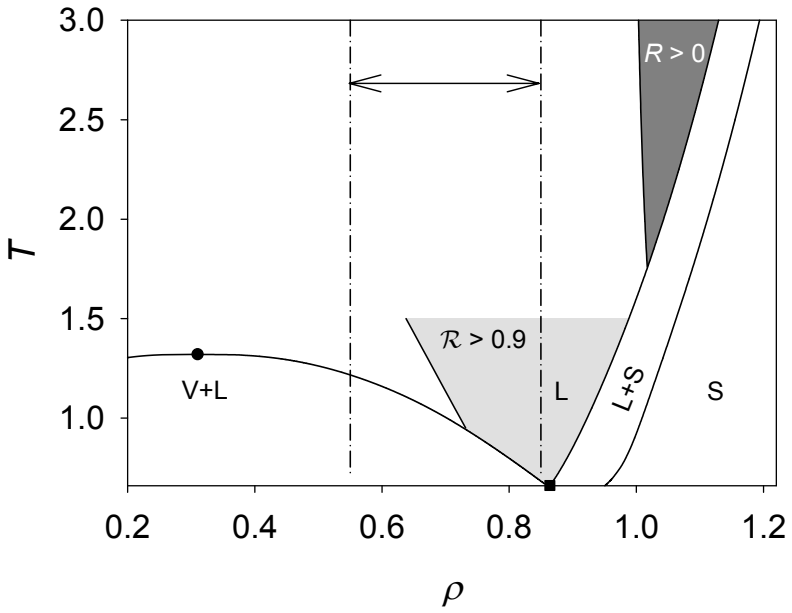

FIG. 1. Density-temperature phase diagram presenting different state regions discussed in the present study: $\mathcal{R} > 0.9$ region adopted from ref. [30] where the isomorph theory may be applied (light grey area); $R > 0$ region where repulsive interparticle interactions dominate (dark grey area), cf. Fig. 12 in section V; region in which the RT temperature scaling analysis for the LJ fluid was performed in ref. [11] (area between the dashed dotted lines); triple point (■); critical point (•) as well as vapor-liquid [31] and liquid-solid (according to eqs. (5), (6)) coexistence curves. S represents the solid, L the liquid state; V+L and L+S are the two-phase regions.

an isomorph, i.e. $s^r = const.$ along the FL. To the best of our knowledge, this conjecture was never assessed. Instead, Pedersen et al. [34] developed an analytical formalism for the FL and ML, assuming that an isomorph may approximate the FL reasonably well. Their results were compared to FL and ML data obtained with the interface pinning simulation method [35] in a region not too close to the triple point.

A goal of the present work was to assess the constancy of the residual entropy s^r along the FL [36]. Following the relations in Table I, the residual entropy s^r was sampled with thermodynamic integration along isochores ranging from $\rho = 0.9$ to 1.7. In addition, s^r was calculated along the FL using saturated densities from empirical correlations recently published by Köster et al. [21]

$$\rho_{\mathrm{FL}} = T^{1/4}[l_0 + l_1 T^{-1} + l_2 T^{-2} + l_3 T^{-3} + l_4 T^{-4} + l_5 T^{-5}] \,, \tag{5}$$

$$\rho_{\mathrm{ML}} = T^{1/4}[s_0 + s_1 T^{-1} + s_2 T^{-2} + s_3 T^{-3} + s_4 T^{-4} + s_5 T^{-5}] \,, \tag{6}$$

with parameters l_i and s_i summarized in Table II. The results are presented in Fig. 2. Moreover, residual entropy

TABLE II. Empirical parameters of correlations (5) and (6) for the coexisting fluid and solid densities of the Lennard-Jones potential taken from ref. [21].

i	l_i	s_i
0	0.794326405787077	0.824314738009423
1	0.287446151493139	0.345860792558053
2	-0.405667818555559	-0.406050983191368
3	0.417645193659883	0.391153270627875
4	-0.211440758862587	-0.164344343309084
5	0.040324958732013	0.018024225929690

data from the recent reference equation of state (EOS) by Thol et al. [31] were compared with the present simulations. Because the EOS was parameterized to a data set in the range $0.7 < T < 9$ and $\rho < 1.08$, a large part of the present simulation data was compared to its extrapolation.

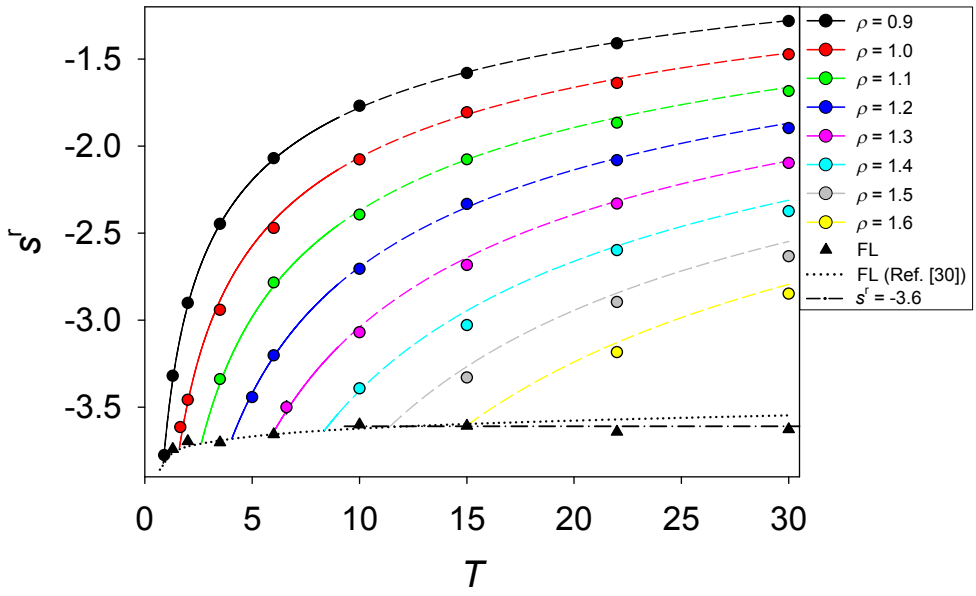

FIG. 2. Residual entropy s^r along isochores in the high density fluid state: EOS by Thol et al. [31] (—), extrapolated (−−) and using (ρ, T) coordinates from eq. (5) to calculate s^r values along the freezing line (···); present simulation data in the fluid phase (•) and along the freezing line (▲); constant residual entropy $s^r = -3.6$ (− · −).

Close to the triple point, s^r strongly depends on temperature, whereas its increase slows down as the temperature continues to rise. In this region, the agreement with the EOS by Thol et al. [31] is excellent. Slight deviations occur when the isochores approach the FL because this region is beyond the specified validity limit of the EOS. However, the results for s^r are consistent. The simulation data along the FL indeed exhibit an almost constant plateau of

approximately $s^r \approx -3.6$ at very high temperatures $T > 10$. For $T < 10$, the residual entropy at the FL decreases gradually with decreasing temperature.

Various entropy-based freezing criteria can be found in the literature. Rosenfeld [37] developed one, finding a residual entropy of $s^r = -4$ for all inverse-power and Yukawa fluids. Chakraborty and Chakravarty [38] determined the two-body entropy s_2 for the LJ, smoothed LJ and Morse potential at the freezing transition. They found that these liquids have values of $s_2 = -3.5 \pm 0.3$ at freezing. May and Mausbach [39] showed that these values also hold for the residual entropy s^r. The entropy values at freezing in the entire temperature range depicted in Fig. 2 belong to this interval. The present results therefore suggest that an isomorphic approximation of the FL should work well in a range $T \geq 10$ for the LJ system. This confirms the findings of Heyes and Brańka [40], who analyzed the FL and ML of the LJ system for $T < 10$. They showed that the isomorphic state evolves gradually with temperature, i.e., the LJ system is only *locally isomorphic* for temperatures $T < 10$.

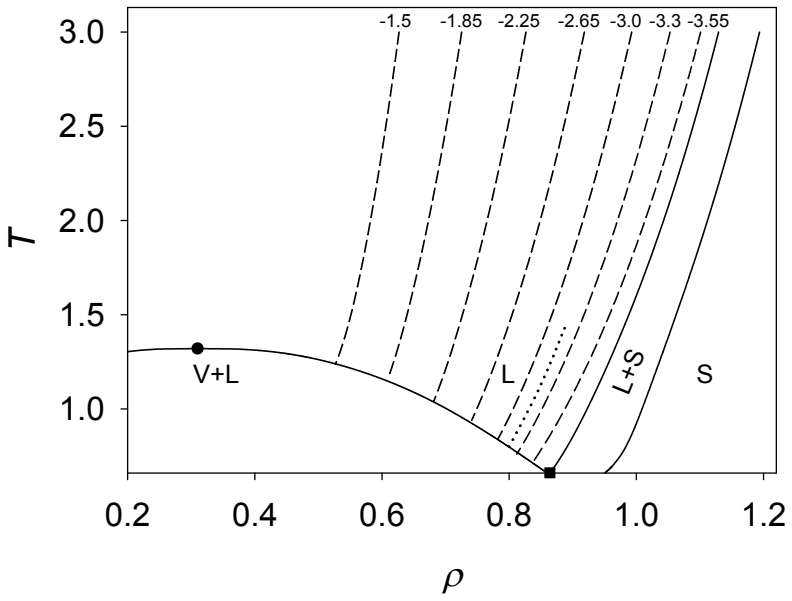

FIG. 3. Isomorphs (configurational adiabats) obtained from the EOS by Thol et al. [31] (−−) ranging from $s^r = -1.5$ to -3.55 as well as a configurational adiabat digitized from ref. [30] (· · ·); triple point (■), critical point (•) as well as vapor-liquid [31] and liquid-solid coexistence curves according to eqs. (5) and (6). S represents the solid, L the liquid state; V+L and L+S are the two-phase regions.

The good agreement between s^r results obtained from thermodynamic integration and the EOS by Thol et al.

[31] allows for a direct representation of isomorphs. In Fig. 3, isomorphs (configurational adiabats) are traced out in the fluid region at constant residual entropy between $s^r = -1.5$ and -3.55. The course of the isomorphs reveals an approach to the FL at higher temperatures that is consistent with the discussion above. The isomorphs slightly diverge from the FL at lower temperatures and the configurational adiabat taken from ref. [30] follows the general trend of the present data.

Other thermodynamic quantities, such as the Helmholtz energy and its volume derivatives, do not belong to the group of invariant properties along isomorphs. Since the isochoric heat capacity c_v is a second-order temperature derivative of the Helmholtz energy, constancy of c_v along isomorphs was postulated in a first version of that theory [41]. However, in a more recent formulation [33], small variations of the isochoric heat capacity c_v were found along isomorphs. An examination of this finding is shown in Fig. 4. The isochoric heat capacity along isochores decreases monotonically with increasing temperature. Along the FL and ML, c_v increases gradually over the entire temperature range, which confirms ref. [33]. An almost constant deviation of the simulation data from the EOS by Thol et al. [31] was observed along the FL.

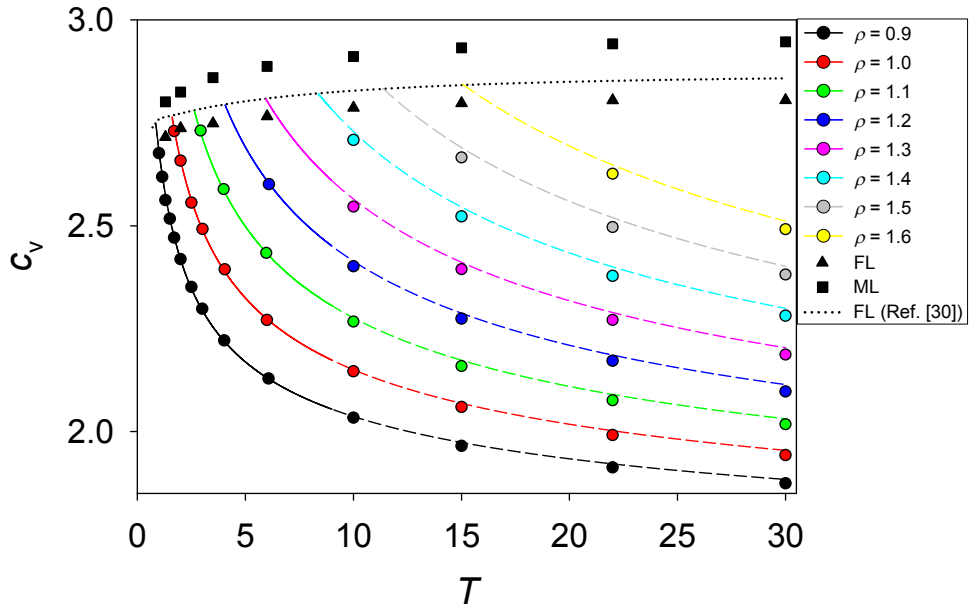

FIG. 4. Isochoric heat capacity c_v along isochores in the high density fluid state: EOS by Thol et al. [31] (—), extrapolated (−−) and using (ρ, T) coordinates from eq. (5) to calculate c_v values along the FL $(\cdots)$; present simulation data in the fluid phase (●) as well as along the FL (▲) and ML (■).

Another important quantity is the scaling exponent

$$\Gamma = \left(\frac{d \ln T}{d \ln \rho}\right)_{\mathrm{FL,ML}} , \tag{7}$$

along the fluid-solid transition. Gilvarry [42] derived

$$\Gamma = 2\,(\gamma_{\mathrm{G}} - \frac{1}{3}) , \tag{8}$$

relating the saturated density dependence on temperature to the Grüneisen parameter γ_{G} [43]. Expression (8) is also known as Lindemann-Gilvarry exponent $\gamma_{\mathrm{LG}} = \Gamma = 2\,(\gamma_{\mathrm{G}} - 1/3)$, which is widely used in geophysics [44]. However, this approach was often called into question so that improvements were attempted. E.g., Stevenson [45] derived an equation for the ML from liquid state theory

$$\Gamma = \left(\gamma_{\mathrm{G}} - \frac{1}{c_v}\right) \Big/ \left(1 - \frac{3}{2\,c_v}\right) . \tag{9}$$

For classical monatomic systems, the right hand side of eq. (9) corresponds to the density scaling exponent γ (cf. Table I), i.e. $\Gamma = \gamma$. Within the Dulong-Petit approximation $c_v = 3$, the density scaling exponent corresponds to the Lindemann-Gilvarry scaling parameter, i.e. $\gamma = \gamma_{\mathrm{LG}}$. Fig. 5 presents the scaling exponent Γ and the density scaling exponent γ along the FL and ML as well as the Lindemann-Gilvarry scaling parameter γ_{LG} along the ML. Throughout, Γ decreases monotonically with increasing temperature, but the expected constant value of $\Gamma = 4$ [2] is approached only at extremely high temperatures. All models seem to asymptotically reach this value, but differences clearly stand out elsewhere. Because the model of Stevenson [45] is based on liquid state theory, it can be expected that it should be more appropriate along the FL. This is indeed the case since the density scaling exponent γ along the FL comes close to the according Γ values also at lower temperatures.

IV. ROSENFELD-TARAZONA TEMPERATURE SCALING

In 1998, RT [4] proposed an equation for the temperature and density dependence of the residual internal energy u^r of classical fluids in the asymptotic high density limit of the form

$$u^r(\rho, T) = u_0^r(\rho) + \alpha(\rho)\, T^{3/5} , \tag{10}$$

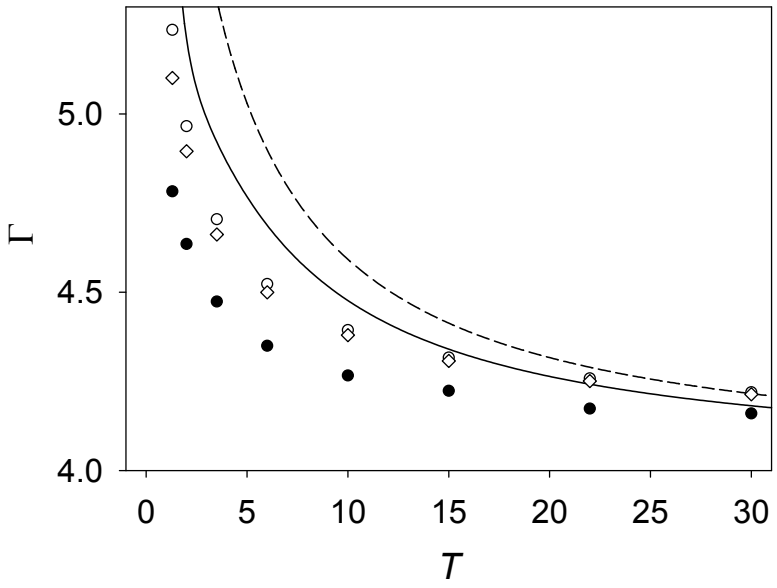

FIG. 5. Scaling exponent Γ along the FL (—) and ML (−−) according to eqs. (5) and (6); simulation data of the density scaling exponent γ along the FL (○) and ML (◇) as well as the Lindemann-Gilvarry scaling parameter γ_{LG} along the ML (●).

where $u_0^r(\rho)$ was termed as Madelung energy [4]. Straightforwardly, the residual isochoric heat capacity $c_v^r = (\partial u^r/\partial T)_v$ is

$$c_v^r(\rho,T) = 3/5\ \alpha(\rho) T^{-2/5}\ , \tag{11}$$

which implies

$$s^r(\rho,T) = s_0^r(\rho) - 3/2\ \alpha(\rho)\ T^{-2/5}\ , \tag{12}$$

since $c_v^r = T(\partial s^r/\partial T)_v$. The applicability of the RT expressions has been verified in the literature for a large number of model systems, such as single-component atomic fluids [4, 38, 39], binary mixtures [46], ionic substances [47] and hydrogen-bonding liquids [48]. In a recent study, Ingebrigtsen et al. [11] analyzed isochoric heat capacity data for 18 model systems and applied statistical measures to assess the RT expressions. These measures were compared with $\mathcal{R}(\rho,T)$, cf. eq. (4), leading to the general statement that the RT expressions are valid for liquids with strong correlations between equilibrium fluctuations of the residual internal energy and virial, i.e., for Roskilde-simple liquids. Nevertheless, Ingebrigtsen et al. [11] reported for the residual isochoric heat capacity of argon an offset of eq. (11),

such that $c_v^r(\rho,T) = \varepsilon(\rho) + 3/5\ \alpha(\rho)T^{-2/5}$, where $\varepsilon(\rho) \neq 0$ indicates poor performance of this RT expression. The cause of this behavior was not further investigated. Experimental data for argon were analyzed for isochores between $\rho = 20$ mol/L and 35 mol/L, which corresponds to a region between the critical density (13.41 mol/L) and the triple point liquid density (35.465 mol/L) [49]. A comparable behavior can also be found for other substances, e.g. for the LJ fluid for isochores between $\rho = 0.55$ and 0.85, being also between the critical density (0.31) and the triple point liquid density (0.86), cf. Fig. 1. It is thus of some interest to investigate the RT expressions in more detail.

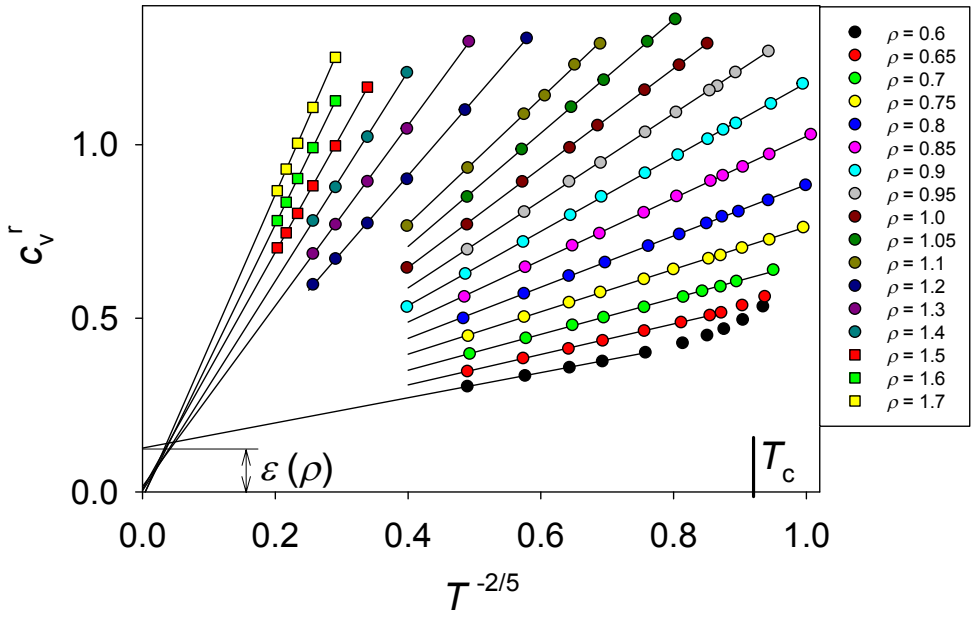

FIG. 6. Residual isochoric specific heat c_v^r along isochores between $\rho = 0.6$ and 1.7: Present simulation data in the fluid state (•); linear regression of simulation data, assessing the RT power-law exponent (—). Note the horizontal $T^{-2/5}$ scale of the plot, where T_c stands for the critical temperature.

Fig. 6 presents simulation results for the residual isochoric heat capacity along isochores as a function of temperature scaled by $T^{-2/5}$. These data were fitted by means of linear regression to assess the RT power-law exponent $-2/5$. It can clearly be seen that this particular RT expression is not satisfied at densities of $\rho = 0.6$ and 0.65 for low temperatures (high $T^{-2/5}$ values). Furthermore, extending the straight lines down to $T^{-2/5} = 0$ ($T \to \infty$) exhibits in the above-mentioned offset $\varepsilon(\rho) \neq 0$. The term $\varepsilon(\rho)$ roughly disappears for isochores $\rho \geq 1.3$. Its density dependence is presented in Fig. 7, showing that it has a maximum close to the triple point, which is in the state region analyzed

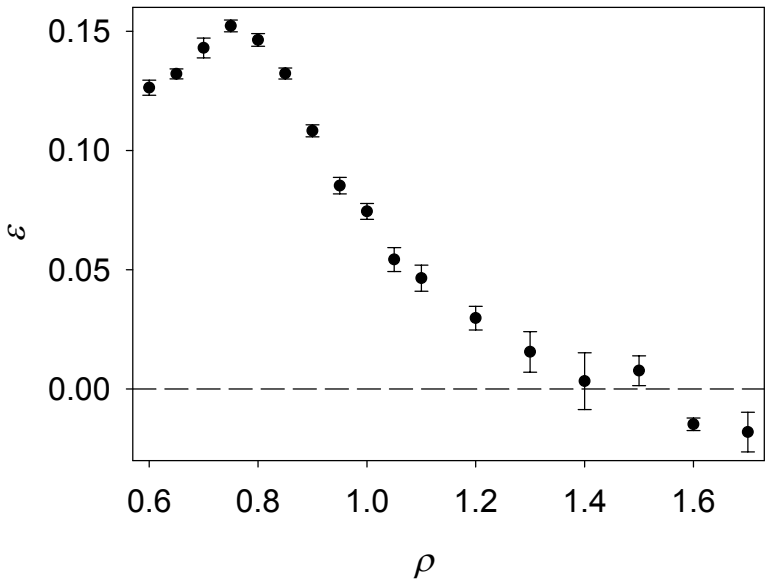

FIG. 7. Density dependence of the $\varepsilon(\rho)$ term based on present simulation data.

in ref. [11]. Having the approximative character of the RT approach in mind and considering the error bounds in Fig. 7, it may be concluded that the offset $\varepsilon(\rho)$ is roughly negligible only for very high densities $\rho \geq 1.3$.

In addition, simulation data for the scaling behavior of the residual entropy s^r are shown in Fig. 8 along isochores, depending on temperature scaled by $T^{-2/5}$. s^r was fitted by means of linear regression in order to assess the RT power-law exponent $-2/5$. In the density range $\rho = 0.9$ to 1.7, the consistency between the straight lines and the simulation data is good. Moreover, the regression fits almost collapse to a single straight line of the form $s^r = -0.4412 - 3.2142\,[T/T_{\rm F}(\rho)]^{-2/5}$ for densities $\rho \geq 1.2$, if $T_{\rm F}(\rho)$ is calculated according to eq. (5), cf. Fig. 9. At freezing, $T = T_{\rm F}(\rho)$, this relation yields $s^r \approx -3.65$, which is very close to the freezing entropy for $T > 10$ discussed in Fig. 2.

The scaling behavior of the residual internal energy u^r is shown in Fig. 10 along isochores, depending on the temperature scaled with $T^{3/5}$. u^r was fitted by means of linear regression in order to assess the Rosenfeld-Tarazona power-law exponent 3/5. The consistency between the straight lines and the simulation data is good. Fig. 11 (top) shows that the density dependent Madelung energy u_0^r exhibits a pronounced minimum at $\rho \approx 1.2$. The density range

where $\frac{d\,u_0^r}{d\,\rho} > 0$ roughly corresponds to the region of good applicability of the Rosenfeld-Tarazona approach ($\rho \geq 1.3$), cf. Fig. 11 (bottom). The coefficient $\alpha(\rho)$ obtained from regression of eqs. (10) to (12) is presented in Fig. 11 (bottom). Data obtained from the residual entropy closely follow values calculated from the residual internal energy. However, data for $\alpha(\rho)$ values obtained from the residual isochoric heat capacity exhibit a systematic deviation to the other two curves at lower densities. This clearly indicates the inconsistency of eqs. (10) to (12) in this region. Accepting small scatter at high densities, data for $\alpha(\rho)$ derived from all three properties are approximately the same for densities $\rho \geq 1.3$.

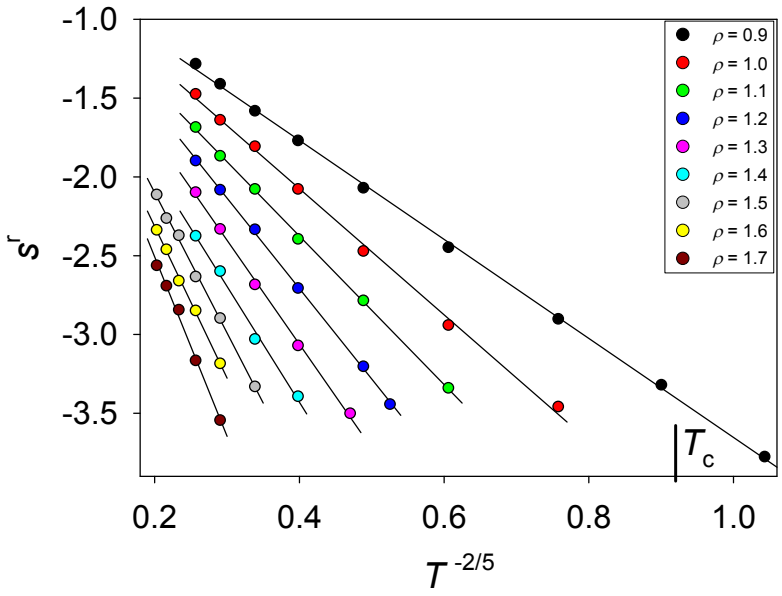

FIG. 8. Residual entropy s^r along isochores between $\rho = 0.9$ and 1.7: Present simulation data in the fluid phase (•); linear regressions of simulation data, assessing the RT power-law exponent (—). Note the horizontal $T^{-2/5}$ scale of the plot, where T_c stands for the critical temperature.

Obviously, the RT expressions are only applicable for densities $\rho \geq 1.3$. If these equations are analyzed close to the triple point liquid density or below, a comparison with the correlation coefficient $\mathcal{R}(\rho, T)$ is problematic. These findings are not surprising because the RT relations were derived from thermodynamic perturbation theory using a hard-sphere reference. In this context, RT originally argued [4] that "*the leading term* [$T^{3/5}$ in eq. (10)], *after the Madelung term, of the asymptotic expansions for the fluid, provides a good estimate of the thermal energy near freezing densities only for predominant repulsive interactions*". To specify this statement in terms of applicability of the RT

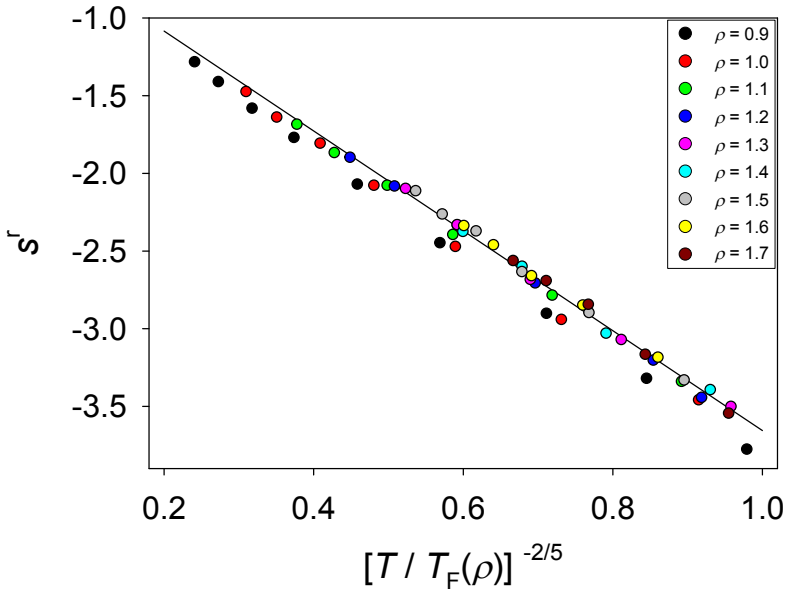

FIG. 9. Residual entropy s^r depending on $(T/T_{\rm F}(\rho))^{-2/5}$, with $T_{\rm F}(\rho)$ according to eq. (5). For $\rho \geq 1.2$ the present simulation data almost collapse to a single straight line of the form $s^r = -0.4412 - 3.2142[T/T_{\rm F}(\rho)]^{-2/5}$.

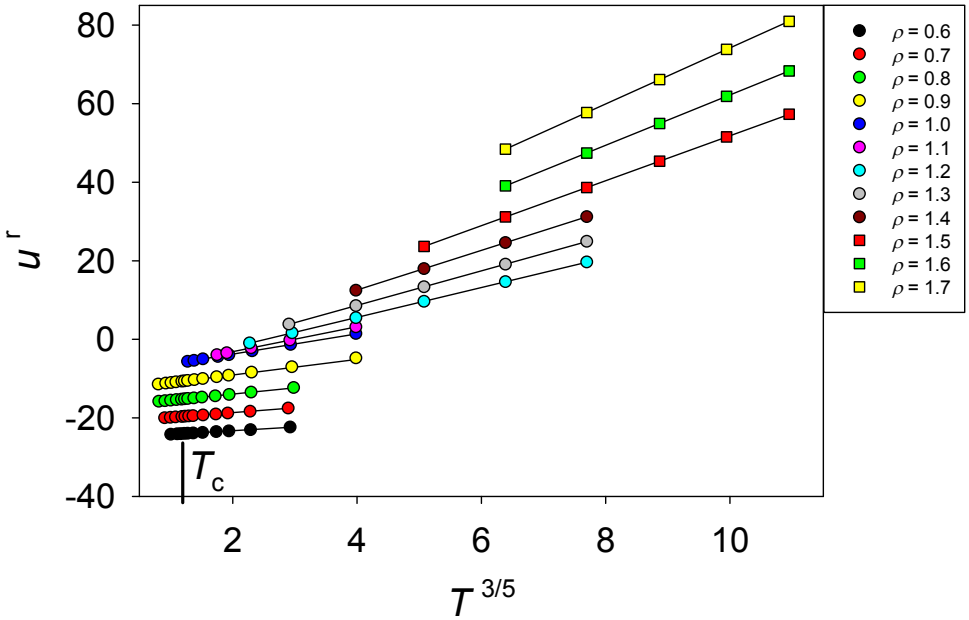

FIG. 10. Residual internal energy u^r: Present simulation data in the fluid phase along isochores between $\rho = 0.6$ and 1.7 (•); linear regression of the individual isochores (—) assessing the Rosenfeld-Tarazona power-law exponent. For visibility reasons, the isochores at $\rho = (0.6, 0.7, 0.8, 0.9)$ were shifted by $\Delta u^r = (-20, -15, -10, -5)$. Note the horizonal $T^{3/5}$ scale of the plot, where $T_{\rm c}$ stands for the critical temperature.

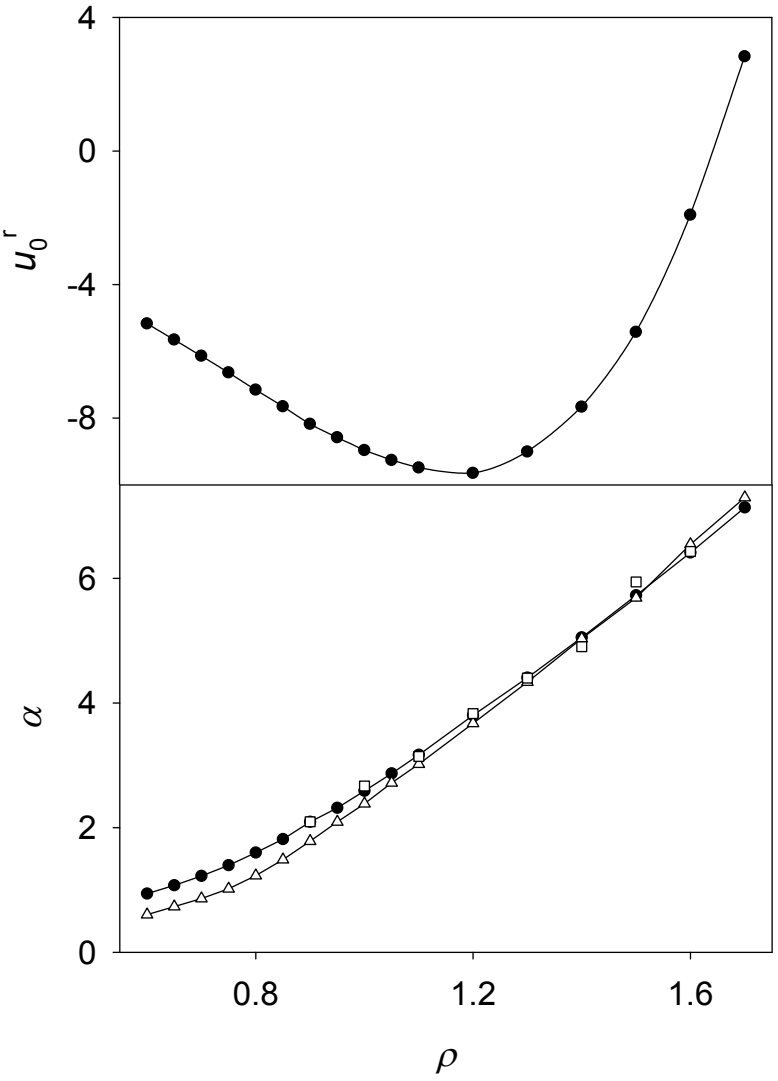

FIG. 11. Madelung energy u_0^r (top) obtained from regression of simulation data for the residual internal energy according to eq. (10). Coefficient $\alpha(\rho)$ (bottom) obtained from regression of simulation data for the residual internal energy (•), residual isochoric heat capacity (△) and residual entropy (□) according to eqs. (10) to (12). The lines are a guide to the eye.

approach and isomorph theory, a criterion is necessary to separate state regions of dominating attractive or repulsive interparticle interactions. The Fisher-Widom line [50] allows for the definition of a boundary between regimes of monotonic/oscillatory long-range decay of the pair correlation function $g(r)$, corresponding to attractive/repulsive interparticle interactions. However, a more natural quantity, which serves as a geometric measure of the interaction strength, is the Riemannian scalar curvature R.

V. THERMODYNAMIC GEOMETRY

In a series of papers [5, 51–57], Ruppeiner and coworkers have shown that fundamentally new insights into the behavior of fluids can be obtained when the Riemannian geometry is introduced in equilibrium thermodynamics. The Riemannian thermodynamic scalar curvature R serves as the key quantity in this concept. An important outcome of this theory is that R is a measure of the interaction strength [13], where the sign of R specifies whether interparticle interactions are effectively attractive ($R < 0$) or repulsive ($R > 0$) according to the curvature sign convention of Weinberg [58]. Its magnitude $|R|$ can be interpreted as a measure of the size of mesoscopic structures in a fluid. For most substances in the fluid phase, the average molecular separation distances are sufficiently large so that attractive interparticle interactions dominate. Consequently, most fluid states exhibit negative R. Attractive interactions also dominate near the critical point, where R diverges to negative infinity. For systems without interparticle interactions, such as the ideal gas, $R = 0$. Nevertheless, fluid states with positive R do exist, typically at high density near the FL as solid-like states [5].

The characteristics of this approach allow for the identification of state regions in which repulsive interactions dominate by identifying a curve $R = 0$. In analogy to the determination of thermodynamic properties based on the Helmholtz energy, the basis of the analysis of R in the present study was the Helmholtz energy $A(T, N, V)$ per volume

$$f = \frac{A}{V} \,, \tag{13}$$

which is associated with the molar Helmholtz energy a by $f = \rho\, a$. Using (ρ, T) coordinates as state variables, the thermodynamic metric is diagonal and its elements are

$$g_{TT} = -\frac{1}{T}\,\frac{\partial^2 f}{\partial T^2} \,, \tag{14}$$

$$g_{\rho\rho} = \frac{1}{T}\,\frac{\partial^2 f}{\partial \rho^2} \,. \tag{15}$$

The determinant g of the metric tensor becomes

$$g = g_{TT}\; g_{\rho\rho} \,, \tag{16}$$

and the Riemannian thermodynamic scalar curvature R is [12]

$$R = \frac{1}{\sqrt{g}} \left[\frac{\partial}{\partial T} \left(\frac{1}{\sqrt{g}} \frac{\partial g_{\rho\rho}}{\partial T} \right) + \frac{\partial}{\partial \rho} \left(\frac{1}{\sqrt{g}} \frac{\partial g_{TT}}{\partial \rho} \right) \right] . \tag{17}$$

The Riemannian thermodynamic scalar curvature R can be calculated from the reference EOS by Thol et al. [31]. Lines of constant curvature in the range of $R = -3.5$ to 0.03 are presented in Fig. 12. Moreover, four curves of constant correlation coefficient $\mathcal{R}$ are shown between $\mathcal{R} = 0.7$ and 0.95. The $\mathcal{R}$ contours were adopted from ref. [30], where they were published only for a relatively small region of the phase diagram. By definition, between the $\mathcal{R} = 0.9$ contour and the FL, the LJ liquid should be Roskilde-simple, i.e. isomorph theory should be applicable, cf. Fig. 1. Despite small inaccuracies due to the scatter of the original $\mathcal{R}$ data in ref. [30], R and $\mathcal{R}$ contour lines were found to be roughly congruent, however, each with a different magnitude. A closer examination of this statement is

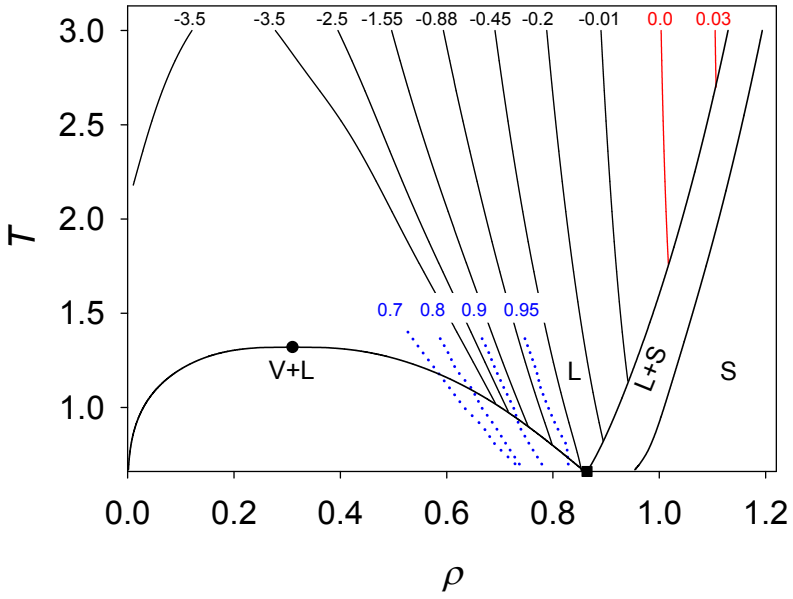

FIG. 12. Contour lines of the Riemannian thermodynamic scalar curvature R for the LJ fluid ranging from R = -3.5 to R = 0.03. The $R \geq 0$ contours are shown in red. Contours of the correlation coefficient $\mathcal{R}$, are shown as dotted blue lines from $\mathcal{R} = 0.7$ to 0.95 which were digitized from ref. [30]. Note that their scatter exists originally in ref. [30] and that the $\mathcal{R}$ contours penetrate the metastable liquid region. Triple point (■), critical point (•) as well as vapor-liquid [31] and liquid-solid coexistence curves. S represents the solid, L the liquid state; V+L and L+S are the two-phase regions.

possible if the Riemannian thermodynamic scalar curvature R is calculated along the coordinates of the $\mathcal{R}$ contour lines. Results of these calculations are shown in Fig. 13 for $\mathcal{R} = 0.8, 0.9$ and 0.95. Horizontal lines represent the mean value of curvature data. Along contour lines $\mathcal{R} \geq 0.9$, R is constant. The $\mathcal{R} = 0.8$ contour line penetrates

deeply into the metastable liquid region in which the curvature R decreases strongly. This leads, together with the noisy $\mathcal{R}$ coordinates of ref. [30], to the scatter at $\mathcal{R} = 0.8$. The $R = 0$ line can be found at a density $\rho \simeq 1.02$, cf. Fig. 12, is roughly temperature independent and terminates on the FL at $T \simeq 1.8$. To the right of the $R = 0$ line, characterized by a dark grey area in Fig. 1, solid-like states are present that are dominated by repulsive interactions ($R > 0$). To the left of the $R = 0$ line, fluid-like states are present, dominated by attractive interactions ($R < 0$). The $R > 0$ region tightly encloses the state region where $\mathcal{R} = 1$ [59, 60], which, in the terminology of isomorph theory, corresponds to a perfectly correlating system.

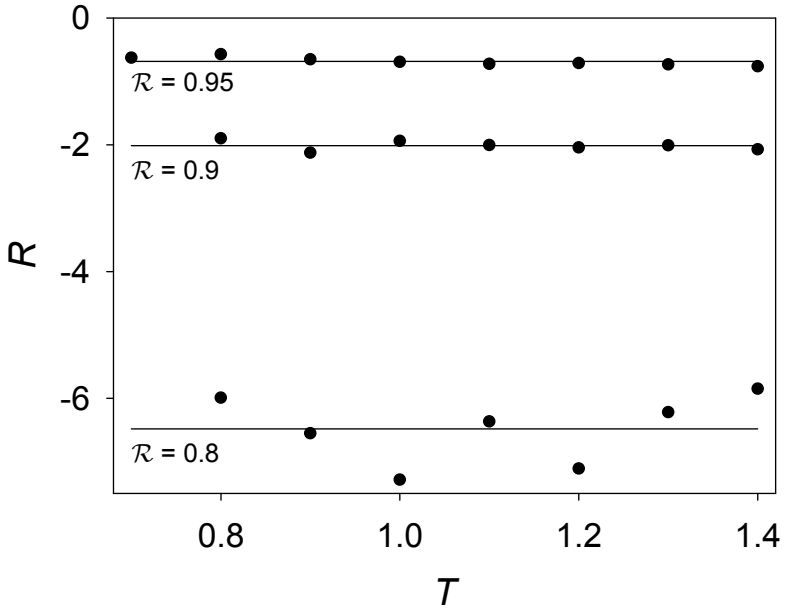

FIG. 13. Riemannian thermodynamic scalar curvature R calculated from the EOS by Thol et al. [31] along the (ρ, T) coordinates of the $\mathcal{R}$ contours at $\mathcal{R} = 0.8, 0.9$ and 0.95.

The scalar curvature R along the FL is shown in Fig. 14, where a sign change at $T \simeq 1.8$ is evident. For $T < 1.8$, R decreases strongly upon its approach to the triple point. For $T > 6.5$, R seems to reach a constant plateau.

Introducing the Riemannian thermodynamic scalar curvature R into the discussion provides new perspectives on the aspects presented above. In connection with the question whether the FL is an isomorph, its separation depending on temperature seems to be reasonable. When interparticle interactions are effectively attractive ($T < 1.8$), the FL is not an isomorph. The required isomorphic condition of constant residual entropy s^r is reached at about $T \simeq 10$,

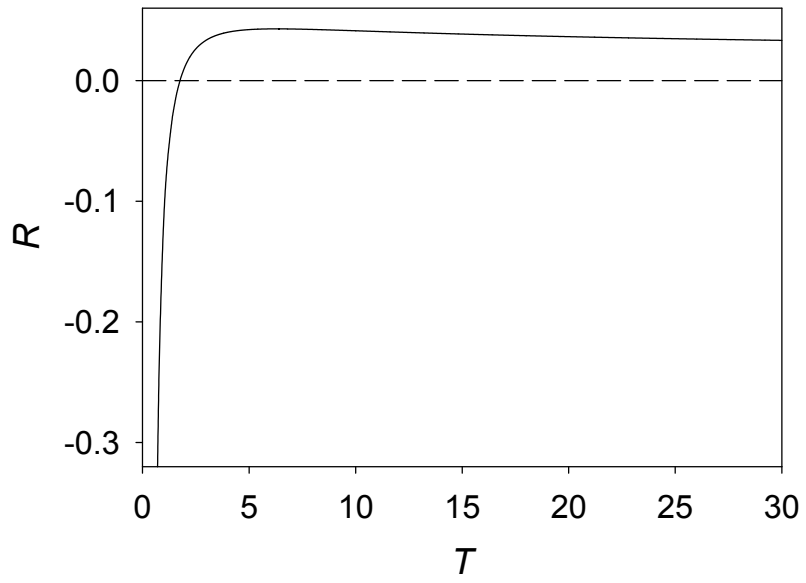

FIG. 14. Riemannian thermodynamic scalar curvature R calculated from the EOS by Thol et al. [31] along the FL.

cf. Fig. 2. In-between, i.e. $1.8 < T < 10$, cf. Fig. 14, the repulsive interaction strength and thus the isomorphic state evolves gradually with temperature, classifying this region in accordance with Heyes and Brańka [40] as *locally isomorphic* only.

These considerations are consistent with the analysis of the RT approach. The RT expressions closely approximate the thermodynamic behavior of the LJ fluid when applied at very high densities of $\rho \gtrsim 1.3$, cf. Fig. 7. This corresponds to a freezing temperature of $T \gtrsim 6.5$, where the repulsive interaction strength has fully developed, cf. Fig. 14. This, in retrospect, confirms the claim of RT.

VI. CONCLUSION

Isomorph theory, RT temperature scaling and Riemannian thermodynamic geometry, describing the behavior of fluids at high densities, were compared with each other on the basis of the LJ potential to explore common physical fundamentals. Partly unproven aspects of isomorph theory were investigated, such as the isomorphic character of the FL and the scaling exponent at freezing and melting. Precise thermodynamic information was provided by means of molecular simulation employing the statistical mechanical formalism of Lustig as well as thermodynamic integration.

Based on the residual entropy, it was established that the FL is an isomorph for temperatures $T \geq 10$. Likewise, different theoretical approaches for the determination of scaling exponents at freezing/melting were analyzed. RT temperature scaling expressions for the residual contributions to internal energy, entropy and isochoric heat capacity were analyzed to investigate discrepancies reported in the literature. The latter is the most sensitive property for exploring this issue. A narrow state region close to the FL was specified, where RT scaling is applicable. Moreover, the Riemannian thermodynamic scalar curvature R was investigated to identify a state region with $R > 0$, where repulsive interactions dominate. Because isomorph theory and RT scaling perform well when repulsive interactions dominate, consistent results from both approaches could be obtained only in this small state region.

Acknowledgments

The authors thank George Ruppeiner for fruitful discussions concerning thermodynamic geometry. Furthermore, the authors gratefully acknowledge the Paderborn Center for Parallel Computing (PC^2) for the generous allocation of computer time on the OCuLUS cluster and computational support by the High Performance Computing Center Stuttgart (HLRS) under the grant MMHBF2. The present research was conducted under the auspices of the Boltzmann-Zuse Society of Computational Molecular Engineering (BZS).

TABLE III. Similar abbreviations used in the literature.

Property	
$\mathcal{R}$	correlation coefficient between residual internal energy and virial
R	Riemannian thermodynamic scalar curvature
R_{G}	ideal gas constant
γ	density scaling exponent
γ_{G}	Grüneisen parameter
γ_{LG}	Lindemann-Gilvarry scaling exponent
Γ	scaling exponent at freezing/melting

APPENDIX A

To avoid confusion between similar abbreviations used in the literature, their meanings are given in Table III.

[1] J. C. Dyre, J. Phys. Chem. B **118**, 10007 (2014).
[2] D. Fragiadakis and C. M. Roland, Phys. Rev. E **83**, 031504 (2011).
[3] D. Bolmatov, V. V. Brazhkin, and K. Trachenko, Nat. Commun. **4**, 2331 (2013).
[4] Y. Rosenfeld and P. Tarazona, Mol. Phys. **95**, 141 (1998).
[5] G. Ruppeiner, P. Mausbach, and H.-O. May, Phys. Lett. A **379**, 646 (2015).
[6] N. P. Bailey, U. R. Pedersen, N. Gnan, T. B. Schrøder, and J. C. Dyre, J. Chem. Phys. **129**, 184507 (2008).
[7] N. P. Bailey, U. R. Pedersen, N. Gnan, T. B. Schrøder, and J. C. Dyre, J. Chem. Phys. **129**, 184508 (2008).
[8] T. B. Schrøder, N. P. Bailey, U. R. Pedersen, N. Gnan, and J. C. Dyre, J. Chem. Phys. **131**, 234503 (2009).
[9] N. Gnan, T. B. Schrøder, U. R. Pedersen, N. P. Bailey, and J. C. Dyre, J. Chem. Phys. **131**, 234504 (2009).
[10] D. Bolmatov, M. Zhernenkov, D. Zavyalov, S. N. Tkachev, A. Cunsolo, and Y. Q. Cai, Sci. Rep. **5**, 15850 (2015).
[11] T. S. Ingebrigtsen, A. A. Veldhorst, T. B. Schrøder, and J. C. Dyre, J. Chem. Phys. **139**, 171101 (2013).
[12] G. Ruppeiner, Rev. Mod. Phys. **67**, 605 (1995), and Erratum **68**, 313, 1996.
[13] G. Ruppeiner, Am. J. Phys. **78**, 1170 (2010).
[14] G. Rutkai, M. Thol, R. Span, and J. Vrabec, Mol. Phys. **115**, 1104 (2016).
[15] A. Lotfi, J. Vrabec, and J. Fischer, Mol. Phys. **76**, 1319 (1992).
[16] M. Heinen, J. Vrabec, and J. Fischer, J. Chem. Phys. **145**, 081101 (2016).
[17] M. Horsch, J. Vrabec, and H. Hasse, Phys. Rev. E **78**, 011603 (2008).
[18] M. Horsch, J. Vrabec, M. Bernreuther, S. Grottel, G. Reina, A. Wix, K. Schaber, and H. Hasse, J. Chem. Phys. **128**, 164510 (2008).
[19] G. A. Fernandez, J. Vrabec, and H. Hasse, Fluid Phase Equilib. **221**, 157 (2004).
[20] J. Vrabec, G. K. Kedia, G. Fuchs, and H. Hasse, Mol. Phys. **104**, 1509 (2006).
[21] A. Köster, P. Mausbach, and J. Vrabec, J. Chem. Phys. **147**, 144502 (2017).
[22] R. Lustig, Mol. Sim. **37**, 457 (2011).
[23] R. Lustig, Mol. Phys. **110**, 3041 (2012).
[24] R. Span, *Multiparameter Equations of State: An Accurate Source of Thermodynamic Property Data* (Springer Verlag, Berlin, 2000).
[25] S. Deublein, B. Eckl, J. Stoll, S. V. Lishchuk, G. Guevara-Carrion, C. W. Glass, T. Merker, M. Bernreuther, H. Hasse, and J. Vrabec, Comput. Phys. Commun. **182**, 2350 (2011).
[26] C. W. Glass, S. Reiser, G. Rutkai, S. Deublein, A. Köster, G. Guevara-Carrion, A. Wafai, M. Horsch, M. Bernreuther, T. Windmann, H. Hasse, and J. Vrabec, Comput. Phys. Commun. **185**, 3302 (2014).
[27] G. Rutkai, A. Köster, G. Guevara-Carrion, T. Janzen, M. Schappals, C. W. Glass, M. Bernreuther, A. Wafai, S. Stephan, M. Kohns, S. Reiser, S. Deublein, M. Horsch, H. Hasse, and J. Vrabec, Comput. Phys. Commun. **221**, 343 (2017).
[28] D. Frenkel and B. Smit, *Understanding Molecular Simulation: From Algorithms to Applications* (Elsevier, San Diego, 2001).
[29] Note that $w = R_{\mathrm{G}}\,T\,A^{\mathrm{r}}_{01}$ and $u^r = R_{\mathrm{G}}\,T\,A^{\mathrm{r}}_{10}$.
[30] N. P. Bailey, L. Bøhling, A. A. Veldhorst, T. B. Schrøder, and J. C. Dyre, J. Chem. Phys. **139**, 184506 (2013).
[31] M. Thol, G. Rutkai, A. Köster, R. Lustig, R. Span, and J. Vrabec, J. Phys. Chem. Ref. Data **45**, 023101 (2016).
[32] In isomorph theory, the term excess is commonly used instead of residual.
[33] T. B. Schrøder and J. C. Dyre, J. Chem. Phys. **141**, 204502 (2014).
[34] U. R. Pedersen, L. Costigliola, N. P. Bailey, T. B. Schrøder, and J. C. Dyre, Nature Commun. **7**, 12386 (2016).

[35] U. R. Pedersen, F. Hummel, G. Kresse, G. Kahl, and C. Dellago, Phys. Rev. B **88**, 094101 (2013).
[36] Note that s^r is frequently approximated in this context by the two-body entropy $s_2 = -2\pi\rho \int [1-g(r)+g(r)\ln(g(r))]\, r^2\, dr$, based on the radial distribution function $g(r)$.
[37] Y. Rosenfeld, Phys. Rev. E **62**, 7524 (2000).
[38] S. N. Chakraborty and C. Chakravarty, Phys. Rev. E **76**, 011201 (2007).
[39] H.-O. May and P. Mausbach, Fluid Phase Equilibr. **313**, 156 (2012).
[40] D. Heyes and A. Brańka, J. Chem. Phys. **143**, 234504 (2015).
[41] T. S. Ingebrigtsen, L. Bøhling, T. B. Schrøder, and J. C. Dyre, J. Chem. Phys. **136**, 061102 (2012).
[42] J. J. Gilvarry, Phys. Rev. **102**, 308 (1956).
[43] P. Mausbach, A. Köster, G. Rutkai, M. Thol, and J. Vrabec, J. Chem. Phys. **144**, 244505 (2016).
[44] O. L. Anderson, *Equations of state of solids for geophysics and ceramic science* (Oxford University Press, New York, Oxford, 1995).
[45] D. J. Stevenson, Phys. Earth Planet. Interiors **22**, 42 (1980).
[46] Z. Shi, P. G. Debenedetti, F. H. Stillinger, and P. Ginart, J. Chem. Phys. **135**, 084513 (2011).
[47] M. Agarwal, R. Sharma, and C. Chakravarty, J. Chem. Phys. **127**, 164502 (2007).
[48] S. Prasad and C. Chakravarty, J. Chem. Phys. **140**, 164501 (2014).
[49] C. Tegeler, R. Span, and W. Wagner, J. Phys. Chem. Ref. Data **28**, 779 (1999).
[50] M. E. Fisher and B. Widom, J. Chem. Phys. **50**, 3756 (1969).
[51] G. Ruppeiner and J. Chance, J. Chem. Phys. **92**, 3700 (1990).
[52] G. Ruppeiner, A. Sahay, T. Sarkar, and G. Sengupta, Phys. Rev. E **86**, 052103 (2012).
[53] G. Ruppeiner, Phys. Rev. E **86**, 021130 (2012).
[54] H.-O. May and P. Mausbach, Phys. Rev. E **85**, 031201 (2012), and Erratum **86**, 059905 (2012).
[55] H.-O. May, P. Mausbach, and G. Ruppeiner, Phys. Rev. E **88**, 032123 (2013).
[56] H.-O. May, P. Mausbach, and G. Ruppeiner, Phys. Rev. E **91**, 032141 (2015).
[57] G. Ruppeiner, N. Dyjack, A. McAloon, and J. Stoops, J. Chem. Phys. **146**, 224501 (2017).
[58] S. Weinberg, *Gravitation and cosmology* (John Wiley and Sons, New York, 1972).
[59] L. Bøhling, N. P. Bailey, T. B. Schrøder, and J. C. Dyre, J. Chem. Phys. **140**, 124510 (2014).
[60] L. Costigliola, T. B. Schrøder, and J. C. Dyre, Phys. Chem. Chem. Phys. **18**, 14678 (2016).